Multiple Cutoff Wave Numbers of the Ablative Rayleigh-Taylor Instability

The Rayleigh-Taylor instability occurs at the interface between heavy and light fluids when the heavy fluid is accelerated by the light fluid. The classical treatment of a sharp interface shows that a small perturbation at this boundary will grow as $e^{\gamma t}$, where γ is the linear growth.[1] The ablation front of an inertial confinement fusion (ICF) imploding target is subject to this instability because the compressed target is accelerated by the low-density ablating plasma. If small perturbations caused by either target imperfections or illumination nonuniformity grew classically, then these small perturbations would grow to sufficient amplitudes to destroy the shell of the target and degrade the performance of the implosion. It has recently been shown by several authors[2–9] that the ablation process will actually reduce the Rayleigh-Taylor growth rate at this interface and can, in fact, stabilize the interface at sufficiently short wavelengths. Calculations of the cutoff wave number for a diffuse density profile were carried out by Kull[7] and by Bud'ko and Liberman.[8] Using the assumption that the cutoff occurs at wavelengths shorter that the density-gradient scale length $L = \left[(1/\rho)(d\rho/dy)\right]^{-1}$, Bud'ko and Liberman[8] used the geometrical optics approximation of the Wentzel-Kramers-Brillouin (WKB) theory to derive the cutoff wave number in the limit of $V_a/\sqrt{gL} \rightarrow 0$, where V_a is the ablation velocity of the overdense portion of the target.

The role of the parameter $\Sigma = V_a/\sqrt{gL}$ can be easily deduced by using the following intuitive form of the instability growth rate, $\gamma \sim \sqrt{kg/(1 + kL)} - kV_a$. By setting $\gamma = 0$, it is easy to show that for $\Sigma \gg 1$ the cutoff wave number occurs at wavelengths longer than the density-gradient scale length $\left(k_c L \sim 1/\Sigma^2 \ll 1\right)$. On the contrary, for $\Sigma \ll 1$, the cutoff occurs a wavelength shorter than L $\left(k_c L \sim 1/\Sigma \gg 1\right)$. The relative size of the cutoff wavelength to the density-gradient scale length suggests the type of mathematical technique that must be used. It is well known that short-wavelength modes with $k_c L \gg 1$ can be investigated using the WKB approximation, and long-wavelength modes $\left(k_c L \ll 1\right)$ have a characteristic "boundary layer" structure in the sharp gradient region and can be studied with a sharp boundary model.

In this article, we derive the physical optics approximation of the WKB theory applied to the ablative Rayleigh-Taylor instability for $\Sigma \ll 1$, and we show the existence of multiple branches in the instability spectrum. Each branch has a different cutoff wave number and an eigenfunction characterized by a different number of zeros. Furthermore, since in typical ICF targets the density profiles are rather steep (direct drive) or the ablation velocity is rather large (indirect drive), the parameter $V_a/\sqrt{gL}$ is only approximately less than 1. The physical optics approximation also provides the next-order correction (in $V_a/\sqrt{gL} < 1$) to the largest cutoff wave number.

The WKB Approximation

We consider an equilibrium in the frame of reference of the ablation front with the heavy fluid of density ρ_h moving with velocity $U_h = -V_a e_y$ (Fig. 60.4). The density smoothly varies from ρ_h to a lower value ρ_l, and the velocity increases according to the conservation of mass flow ($\rho U = constant$). The fluid is subject to a force field $g = g e_y$ opposite to the density gradient ($g < 0$), and the density profile has a finite density-gradient scale length in the ablation region ($y \approx 0$) with characteristic value L_0 $\left[L(0)/L_0 \sim 1\right]$. To treat the linear stability of ablation fronts, we consider a simplified incompressible model for the perturbation that is valid for subsonic ablation flow ($V_a \ll C_s$, where C_s is the sound speed)

$$\frac{d\rho}{dt} + \rho \mathbf{V} \cdot \mathbf{v} = 0$$

$$\rho \frac{d\mathbf{v}}{dt} = -\nabla p + \rho \mathbf{g} \tag{1}$$

$$\mathbf{V} \cdot (\mathbf{v} - \mathbf{U}) = 0$$

where $\mathbf{U}$ is the equilibrium velocity and $d/dt = \partial/\partial t + \mathbf{v} \cdot \mathbf{V}$.

The set of linearized conservation equations can be written in the following form:
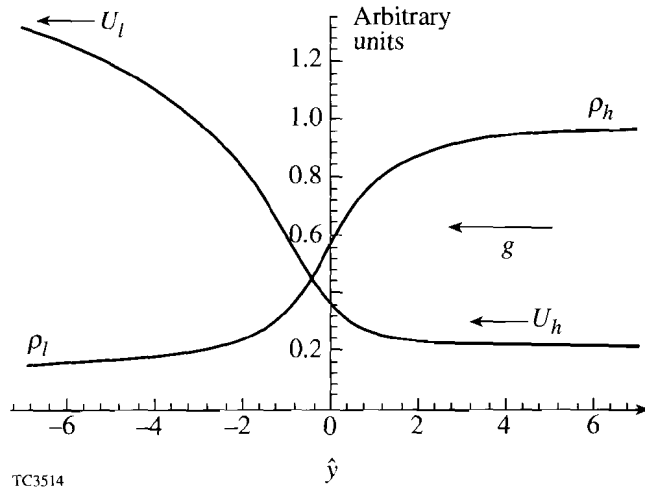
TC3514

Figure 60.4

Density and velocity profiles. The subscripts l and h indicate the light and heavy fluid respectively.

$$\left(\frac{\Gamma}{\epsilon}+\partial_{\hat{y}}\right)\tilde{n} = -\tilde{v}_y / U\hat{L} \qquad (2)$$

$$\left(\frac{\Gamma}{\epsilon}+\partial_{\hat{y}}\right)\tilde{v}_x = -i\tilde{p}/\epsilon\,\rho U \qquad (3a)$$

$$\left(\frac{\Gamma}{\epsilon}+\partial_{\hat{y}}-1/\hat{L}\right)\tilde{v}_y = -\partial_{\hat{y}}(\tilde{p}/\rho U)-\tilde{n}GL_0/U \qquad (3b)$$

$$\partial_{\hat{y}}\tilde{v}_y = -i\tilde{v}_x/\epsilon\,, \qquad (4)$$

where $\epsilon = 1/(kL_0)$, $\hat{y} = y/L_0$, $\tilde{n} = \tilde{\rho}/\rho$, $G = -g - U^2/L$, $\hat{L} = L/L_0$, and $\Gamma = \gamma/kU$. Equations (2)–(4) can be combined into a single fourth-order ordinary differential equation

$$\left(\frac{\Gamma}{\epsilon}+\partial_{\hat{y}}-\alpha/\hat{L}\right)$$

$$\left[\epsilon^4\,\partial_{\hat{y}}\left(\frac{\Gamma}{\epsilon}+\partial_{\hat{y}}\right)\partial_{\hat{y}}\tilde{v}_y - \epsilon^2\left(\frac{\Gamma}{\epsilon}+\partial_{\hat{y}}-1/\hat{L}\right)\tilde{v}_y\right]$$

$$+\tilde{v}_y\sigma^2/\hat{L} = 0, \qquad (5)$$

where $\alpha = -\hat{L}\partial_{\hat{y}}\ln(U/G)$ and $\sigma^2 = G/k^2U^2L_0$. Since Eq. (5) cannot be solved exactly, we look for an approximate solution when the parameter $\Sigma^2 = V_a^2/g\,L_0$ is much less than

unity, and we order $\epsilon \sim \Sigma \ll 1$, $\sigma \sim 1$, $G \simeq -g\left[1+O(\epsilon^2)\right]$, and $\alpha \simeq 1 + O(\epsilon^2)$. The validity of the chosen ordering will be verified *a posteriori*. We apply the WKB theory to the fourth-order equation, and we adopt the following ansatz for the perturbation: $\tilde{v}_y = A(\hat{y})\exp[S(\hat{y})/\epsilon]$, where $A(\hat{y})$ and $S(\hat{y})$ are two slowly varying functions of $\hat{y}$, i.e., $\partial_{\hat{y}}\ln S \sim \partial_{\hat{y}}\ln A \sim 1$. The equation for $S(\hat{y})$ (geometrical optics) can be easily derived by retaining the lowest-order terms (~ 1) in Eq. (5):

$$(S'-\Gamma)^2(S'^2-1)+\sigma^2/\hat{L} = 0. \qquad (6)$$

This equation is identical to the one derived in Ref. 8. By focusing on the mode corresponding to the cutoff wave number k_c $\left[Lim_{k\to k_c}\gamma(k)\to 0^+\right]$, we solve Eq. (6) for $|\Gamma| \ll 1$ and find the four roots

$$S_1 = \left(1/\sqrt{2}\right)\int_{\bar{y}}^{\hat{y}}\left[\left(q^+\right)^{1/2}-\tau^-\right]d\hat{y}$$

$$S_2 = -\left(1/\sqrt{2}\right)\int_{\bar{y}}^{\hat{y}}\left[\left(q^+\right)^{1/2}+\tau^-\right]d\hat{y}$$

$$S_3 = \left(1/\sqrt{2}\right)\int_{\bar{y}}^{\hat{y}}\left[\left(q^-\right)^{1/2}-\tau^+\right]d\hat{y} \qquad (7)$$

$$S_4 = -\left(1/\sqrt{2}\right)\int_{\bar{y}}^{\hat{y}}\left[\left(q^-\right)^{1/2}+\tau^+\right]d\hat{y},$$

where

$$q^{\pm} = 1\pm 2\sqrt{Q}, \qquad \tau^{\pm} = \frac{\Gamma}{\sqrt{2}}\left(1\pm\frac{1}{2\sqrt{Q}}\right), \qquad (8)$$

$Q(\hat{y}) \equiv 1/4 - \sigma^2/\hat{L}$, and $\bar{y}$ is an arbitrary point. Observe that Eqs. (7)–(8) are valid for nonvanishing Q and the small t corrections are important only for $|\hat{y}| \to \pm\infty$, where $q^- \to 0$, and they can be neglected for any other value of $\hat{y}$. If Q vanishes at some point, Eq. (6) can be easily solved in the neighborhood of that point and $\Gamma \to 0^-$ yielding $S \cong \pm(\hat{y}-\bar{y})\sqrt{2}$. This result can also be recovered from Eqs. (7)–(8) by neglecting τ even for $Q \simeq 0$. We emphasize that the parameter τ is important for S_3 and S_4 only when $|\hat{y}| \to \infty$. While in Ref. 8 the analysis is limited to the geometrical optics [Eqs.(6)–(8)], here we extend the solution to include the physical optics approximation. By retaining the ϵ corrections

in Eq. (6), the following expressions for $A(\hat{y})$ are derived:

$$A_1 = a_1 F^+(\hat{y})$$

$$A_2 = a_2 F^+(\hat{y})$$

$$A_3 = a_3 F^-(\hat{y}) \tag{9}$$

$$A_4 = a_4 F^-(\hat{y})$$

$$F^{\pm}(\hat{y}) = \left(\frac{G}{|U|}\right)^{1/4} \frac{1}{Q^{1/4}\left(1 \pm 2\sqrt{Q}\right)^{1/4}} \exp\left[m\frac{3}{8}\int_{\hat{y}}^{\hat{y}} \frac{d\hat{y}}{L\sqrt{Q}}\right]. \tag{10}$$

It is important to recognize that none of the eigenfunctions represented by Eqs. (7)–(10) satisfies the boundary conditions of vanishing amplitude at both $+\infty$ and $-\infty$ simultaneously. This observation is supported by the form of the exponential terms in S_j and A_j and by the asymptotic behavior of $Q(\hat{y})$ [Fig. 60.5(a)]. It is readily derived from Eqs. (7)–(10) that in order to satisfy the boundary conditions at $y \to +\infty$, the coefficients a_1, a_3, a_4 must vanish ($a_1 = a_3 = a_4 = 0$ and $a_2 \neq 0$). On the contrary, to satisfy the boundary condition at $y \to -\infty$, the coefficient a_2 must vanish ($a_2 = 0$). Thus, the solution valid for positive y must be matched to a different solution valid for negative y. The necessary condition for the matching to occur is that $Q(\hat{y})$ vanishes at some point and the A_j's become singular. The solid line of Fig. 60.5(a) represents a possible behavior of $Q(\hat{y})$ that would allow the matching. In general there must be two points (turning points) where Q vanishes ($\hat{y} = \hat{y}_1$ and $\hat{y} = \hat{y}_2$ with $\hat{y}_1 > \hat{y}_2$) and at such points, the WKB approximation breaks down, i.e., the A_j's become singular. By defining $\hat{y}_0$ the point of minimum of

$$Q'(\hat{y}_0) = 0, \quad Q(\hat{y}_0) < 0, \quad Q''(\hat{y}_0) > 0,$$

we order $Q(\hat{y}_0) \sim \epsilon$ and $\hat{y}_1 - \hat{y}_2 \sim \sqrt{\epsilon}$. This ordering is verified later by the matching conditions of the solution between the turning points with the WKB approximations. As shown in Fig. 60.5(b), three regions can be identified: (1) the first outer region for $\hat{y} > \hat{y}_1$, where

$$\tilde{v}_y = A_2(\hat{y}) \exp[S_2(\hat{y})/\epsilon];$$

(2) the second outer region for $\hat{y} < \hat{y}_2$, where

$$\tilde{v}_y = A_1 \exp[S_1/\epsilon] + A_3 \exp[S_3/\epsilon] + A_4 \exp[S_4/\epsilon];$$

and (3) the inner region between the turning points $\hat{y}_2 < \hat{y} < \hat{y}_1$. To determine the solution in the inner region, we look at the behavior of the solution in the first outer region for $\sqrt{\epsilon} \ll \hat{y} - \hat{y}_0 \ll 1$ and approximate Q with its Taylor expansion $Q \approx Q_0 + Q_0''(\hat{y} - \hat{y}_0)^2/2$. By setting $\bar{y} = \hat{y}_0$, a straightforward manipulation yields

(a)

(b)
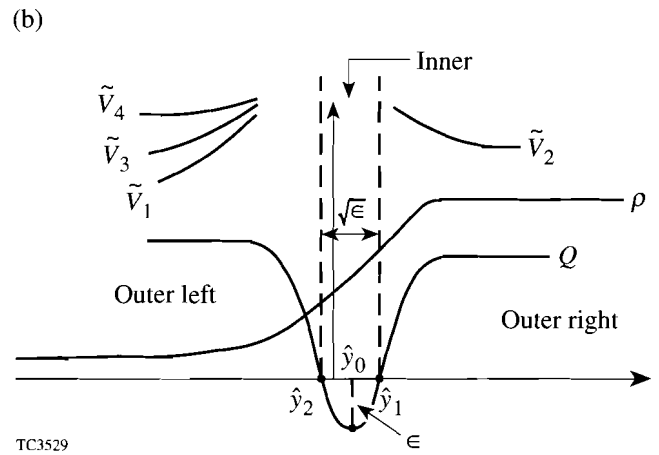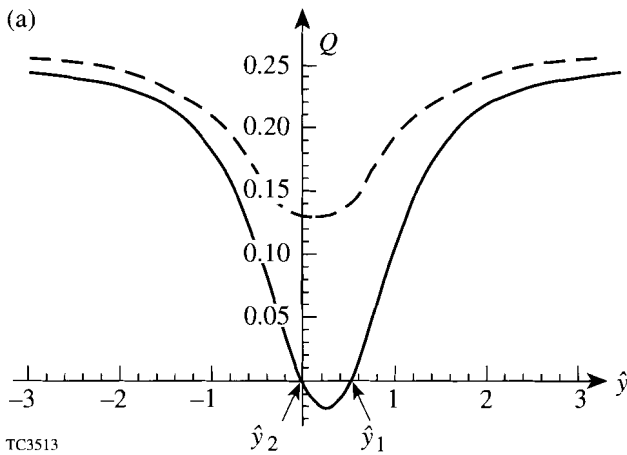
Figure 60.5
(a) Plot of Q versus $\hat{y}$. The dashed line represents a behavior without zeros $\left[(\sigma^2/\hat{L})_{max} < 1/4\right]$. The solid line shows a $Q(\hat{y})$ with two zeros $\left[(\sigma^2/\hat{L})_{max} > 1/4\right]$. For large $|\hat{y}|$, Q approaches $1/4$. (b) Plot of the WKB solutions in the outer regions $\hat{y} \gg \hat{y}_1$ and $\hat{y} \ll \hat{y}_2$.

$$\tilde{v}_y\left(\hat{y} \approx \hat{y}_0^-\right) = \hat{a}_2 \hat{x}^\nu \exp\left[-\frac{1}{4}\sqrt{Q_0''}\,\hat{x}^2\right]\exp\left[-\frac{\left(\hat{y}-\hat{y}_0\right)}{\sqrt{2}\,\epsilon}\right], \quad (11)$$

where $\hat{x} = \left(\hat{y}-\hat{y}_0\right)/\sqrt{\epsilon}$, and

$$\nu = -\frac{1}{\sqrt{Q_0''}}\left(\frac{3}{2^{5/2}\hat{L}(\hat{y}_0)}\right) - \frac{1}{2} - \frac{Q_0}{\sqrt{Q_0''}}\frac{1}{2\,\epsilon} \quad (12)$$

$$\hat{a}_2 = a_2\frac{\sqrt{2}}{Q_0^{1/4}}\left[\frac{G(\hat{y}_0)}{|U(\hat{y}_0)|}\right]^{1/4}\left(\frac{2\,\epsilon\,Q_0''}{Q_0}\right)^{\nu/2}. \quad (13)$$

The function given by Eq. (11) shows a two-scale structure (the two scales being ϵ and $\sqrt{\epsilon}$), different from what is found from the familiar second-order WKB solution near the turning points. Thus, in order to perform the matching, the solution between the turning points must retain the two-scale structure and behave as $\tilde{v}_y = \tilde{u}(\hat{x})\exp\left[-(\hat{y}-\hat{y}_0)/\sqrt{2}\,\epsilon\right]$. Substituting into the general Eq. (6) and retaining the lowest-order terms in ϵ leads to the following equation for $\tilde{u}$:

$$\left[\partial_\xi^2 + \nu + \frac{1}{2} - \frac{1}{4}\xi^2\right]\tilde{u} = 0, \quad (14)$$

where $\xi = \hat{x}\left(Q_0''\right)^{1/4}$. The equation for $\tilde{u}$ is just a second-order equation (instead of fourth order) and can be exactly solved. The solution of Eq. (13) is the combination of two parabolic cylinder functions $\tilde{u} = BD_\nu(\xi) + CD_\nu(-\xi)$. Matching the inner with the outer solution for $\hat{y} > \hat{y}_1$ leads to $C = 0$ and $B = \hat{a}_2/(Q_0'')^{\nu/4}$. To match the rapidly varying exponential $\left\{\exp\left[-(\hat{y}-\hat{y}_0)/\sqrt{2}\,\epsilon\right]\right\}$ of the inner solution with the outer solution in the region $\hat{y} < \hat{y}_2$, the coefficients a_1 and a_3 of the outer solution must vanish. Therefore, as $\hat{y}$ approaches $\hat{y}_2$ $\left(\sqrt{\epsilon} \ll \hat{y}_0 - \hat{y} \ll 1\right)$, the outer solution assumes the following form:

$$\tilde{v}_y\left(\hat{y} \approx \hat{y}_0^+\right) = \hat{a}_4\left(-\hat{x}\right)^\nu \exp\left[-\frac{1}{4}\sqrt{Q_0''}\,\hat{x}^2\right]\exp\left[-\frac{\left(\hat{y}-\hat{y}_0\right)}{\sqrt{2}\,\epsilon}\right], (15)$$

where

$$\hat{a}_4 = a_4\frac{\sqrt{2}}{Q_0^{1/4}}\left[\frac{G(\hat{y}_0)}{|U(\hat{y}_0)|}\right]^{1/4}\left(\frac{2\,\epsilon\,Q_0''}{Q_0}\right)^{\nu/2}. \quad (16)$$

Focusing on the inner solution, the asymptotic behavior of the parabolic cylinder function is easily derived:

$$D_\nu\left(\xi \to -\infty\right) \sim \xi^{-\nu-1}\exp\left[\xi^2/4\right] \qquad \nu \neq n \quad (17a)$$

$$D_n\left(\xi \to -\infty\right) \sim \xi^n\exp\left[-\xi^2/4\right] \qquad \nu = n, \quad (17b)$$

where n is an integer. By matching the inner solution with Eq. (15), we immediately deduce that ν must be an integer $(\nu = n$ with $n = 0, 1, 2 \ldots)$, $a_4 = (-1)^n a_2$, and

$$D_n(\xi) = 2^{-n/2}\exp\left[-\xi^2/4\right]H_n\left[\xi/\sqrt{2}\right]$$

(H_n is the Hermite polynomial). The condition $\nu = n$ represents the equation for the cutoff wave number and can be rewritten in the extended form

$$\frac{Q_0}{\sqrt{Q_0''}}\frac{1}{2\,\epsilon} = -\left(n+\frac{1}{2}\right) - \frac{1}{4\sqrt{2Q_0''}}\frac{3}{\hat{L}(\hat{y}_0)}, \quad (18)$$

where $\epsilon = 1/(k_c L_0)$. Observe that Eq. (18) yields $Q_0 \sim \epsilon$ and $\sigma \sim 1$, in agreement with the initial assumptions. Equation (18) can be solved perturbatively by expanding k_c in powers of $\Sigma < 1$ $(k_c = k_0 - \Sigma k_1 \ldots)$. A short calculation yields the following expression for the cutoff wave number

$$k_c = k_0\left\{1 - \beta\Sigma\left[(2n+1)\sqrt{\frac{d^2Q}{d\hat{y}^2}(\hat{y}_0)} + \frac{3}{2^{3/2}}\frac{1}{\hat{L}(\hat{y}_0)}\right]\right\}, \quad (19)$$

where $k_0 = 2\left[|g|/L(\hat{y}_0)\right]^{1/2}/|U(\hat{y}_0)|$, $\beta = \sqrt{\hat{L}(\hat{y}_0)}\,\rho_h/\rho(\hat{y}_0)$, and $n = 0, 1, 2 \ldots$.

Discussion

The first important result of Eq. (19) is that multiple cutoff wave numbers exist for different values of n. In the γ, k plane, this leads to an unstable spectrum characterized by multiple branches lying one below the other. The branch with the largest cutoff and therefore the largest growth rate is for $n = 0$. Although the lowest-order cutoff wave number k_0 was previously found in Ref. 8, we emphasize the importance of the first-order correction to determine the existence of the multiple branches and to provide a more accurate formula for the $n = 0$ branch when $\Sigma \leq 1$. Table 60.I provides a comparison

between the cutoff wave number of the $n = 0$ branch predicted by Eq. (19) and the one of Ref. 8 for the following form of the density profile

$$\rho(y) = \frac{\rho_h}{1+A}\left[1 + \frac{2}{\pi} A \tan^{-1}\frac{y}{L_0}\right]. \qquad (20)$$

Table 60.I   Cutoff wave number for $n = 0$. Comparison of the cutoff wave number for the $n = 0$ branch predicted by Eq. (19) and Ref. 8 for $A = 0.9$, $g = 5 \times 10^{15}$ cm/s², $v_a = 7.5 \times 10^4$ cm/s, and varying L_0.

L_0 (μm)	Eq. (19) (μm^{-1})	Ref. 8 (μm^{-1})	Σ
50.0	1.05	1.10	0.015
10.0	2.22	2.66	0.034
5.0	2.99	3.48	0.047
3.0	3.68	4.49	0.061
2.0	4.28	5.50	0.075
1.0	5.33	7.78	0.11
0.5	6.10	11.01	0.15

Observe that the first-order correction in Σ becomes important when the density profile is rather steep (direct-drive ICF) or the ablation velocity is rather large (indirect-drive ICF). Since the eigenfunction in the inner region is proportional to $H_n(\xi)$, the integer n determines the number of zeros of the eigenfunction. Figure 60.6 shows the normalized eigenfunction for the $n = 0$, $n = 1$, and $n = 2$ modes for a smooth density profile. Observe the degradation of the matching between the outer WKB approximations and the inner solution as n increases. This effect is due to the increasing magnitude of the higher-order corrective terms that scale as $\Sigma k_1(n)/k_0$. Thus we expect that the matching cannot be performed for $\Sigma k_1(n)/k_0 > 1$ and the number of branches does not exceed N with $\Sigma k_1(N)/k_0 > 1$. Equation (19) has also been solved numerically, and the results have been compared with the analytical predictions. Figure 60.7 shows the unstable spectrum of an equilibrium configuration typical of direct-drive ICF with $g = 5 \times 10^{15}$ cm/s², $V_a = 7.5 \times 10^4$ cm/s, $A = 0.9$, and $L_0 = 2$ μm. Three branches have been found with $n = 0$, $n = 1$, and $n = 2$. For this set of parameters $\Sigma k_1(3)/k_0 = 1.01$, and the predicted number of branches is indeed $N = 3$. Equation (19) predicts the following values of the cutoff wave numbers: $k_c(n = 0) = 4.28$ μm^{-1}, $k_c(n = 1) = 2.83$ μm^{-1}, and $k_c(n = 2) = 1.37$ μm^{-1}. As expected the accuracy of Eq. (19) in predicting the cutoff wave number degrades as n increases. For the same equilibrium parameters, the geometrical optics approximation
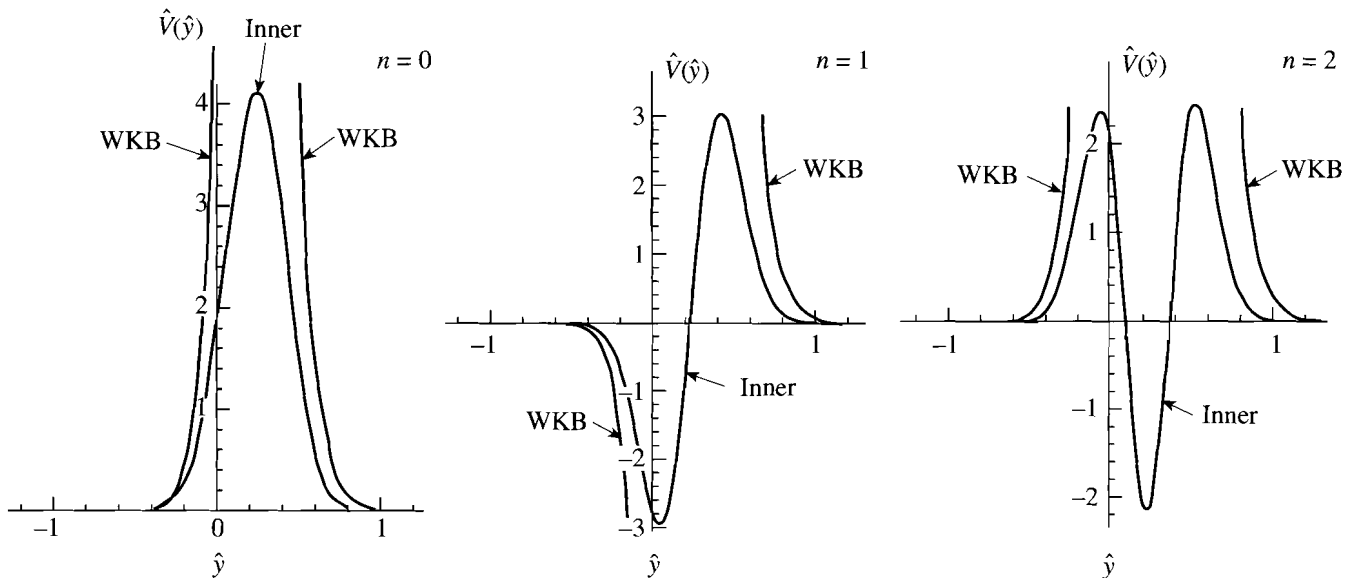
TC3515

Figure 60.6

Plot of the normalized eigenfunction $\hat{V} = \tilde{v}_y(\hat{y})\exp\left[(\hat{y}-\hat{y}_0)/\sqrt{2}\,\epsilon\right]$, for the $n = 0, 1, 2$ modes and the following equilibrium parameters: $A = 0.8$, $g = 10^{15}$ cm/s², $v_a = 10^4$ cm/s, and $L_0 = 10$ μm.

TC3518

$k\,(\mu m^{-1})$ $\blacktriangle$ = theory
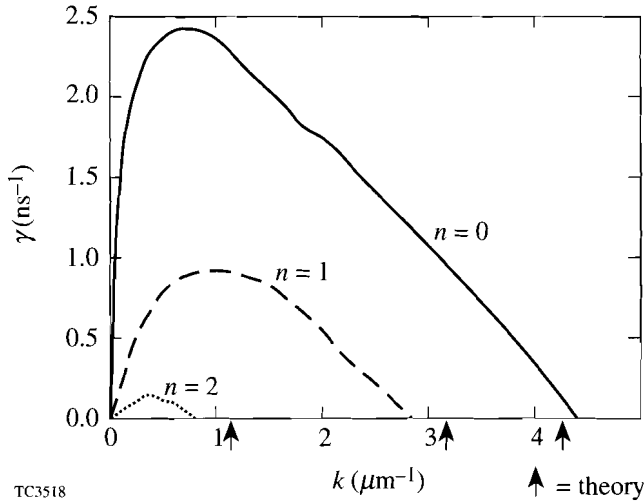
Figure 60.7
Plot of the growth rate versus the wave number for the $n = 0, 1, 2$ branches and the following equilibrium parameters: $A = 0.9$, $g = 5 \times 10^{15}\,cm/s^2$, $v_a = 7.5 \times 10^4\,cm/s$, and $L_0 = 2\,\mu m$.

of Ref. 8 predicts a cutoff of the $n = 0$ mode at $k = 5.5\,\mu m^{-1}$ with a relative error of approximately 30%. To simplify Eq. (19), we focus on typical ICF equilibria with $A \approx 1$ and density profile given by Eq. (20) to determine an approximate value of $\hat{y}_0$, $\hat{y}_0 \approx 0.25\left(\sqrt{8 + \pi^2} - \pi\right)$. Substituting $\hat{y}_0$ into the expressions for $Q(\hat{y}_0)$ and $\hat{L}(\hat{y}_0)$, we derived the following approximate form of the cutoff wave number:

$$k_c \approx k_0\left[1 - 2\sqrt{\pi}\ \Sigma\left(n + \frac{7}{8}\right)\right] \qquad (n = 0, 1, 2 \ ...) \quad (21)$$

and $k_0 \approx \left(\sqrt{2.17/\pi}\right)\big/\Sigma L_0$. In addition to the cutoff wave number, the WKB approximation also provides the position where the short-wavelength modes are localized. The peak of the eigenfunction is located at the point $\hat{y}^*$, where $S'\!\left(\hat{y}^*\right) = 0$. Using Eq. (6) at $\hat{y} = \hat{y}^*$ we derive an equation for $\hat{y}^*$:

$$\Gamma^2\!\left(\hat{y}^*\right) = \sigma\!\left(\hat{y}^*\right)^2\big/\hat{L}\!\left(\hat{y}^*\right). \quad (22)$$

For any given Γ, Eq. (22) can be solved for the unknown $\hat{y}^*$. It follows immediately that the mode corresponding to the cutoff wave number ($\Gamma = 0$) has the peak of the eigenfunction at $-\infty$, where $1/\hat{L} = 0$. More generally, it can be deduced from Eq. (22) that as the wave number of the mode increases and the growth rate decreases, the peak of the eigenfunction is shifted

downstream in the light-fluid region. To verify the accuracy of the incompressible model in predicting the unstable spectrum for $\Sigma < 1$, we compare the growth rates derived from Eqs. (2)–(4) with the numerical results of Ref. 3, where the full set of fluid equations, including thermal transport, has been numerically solved. According to Ref. 3, the growth-rate dependence on the mode wave number is well fit by the following formula:

$$\gamma = 0.9\sqrt{kg} - \beta k V_a, \quad (23)$$

where β is an adjustable parameter varying between 3 and 4. Figure 60.8 shows an unstable spectrum obtained from the numerical solution of the incompressible model for $\Sigma = 0.14$ and Takabe's formula for $\beta = 3$–4. Observe that the predictions of the incompressible model (for $\Sigma < 1$) are in good agreement with the more general results of Ref. 3. For the same value of Σ, Eq. (19) yields the normalized cutoff wave number $\sqrt{k_c V_a^2/g} = 0.26$. To check the validity of the incompressible mode for arbitrary equilibria, we also compare the incompressible spectrum for $\Sigma \gg 1$ with the result of Ref. 3. We find that the incompressible model predicts a larger ablative stabilization than Eq. (23). For $\Sigma \gg 1$, the incompressible growth rate can be written in the following form:

$$\gamma = \sqrt{AKg} - kV_a\frac{1 + A}{1 - A} \quad (24)$$

in agreement with the results of Ref. 4. For $A \approx 1$, Eq. (24) predicts a large stabilization that is not observed in the numerical simulations.[3,5,9] We conclude that the incompressibility assumption breaks down for $\Sigma \gg 1$, and the effect of finite thermal conductivity must be retained.[7]

Conclusions

We have derived the physical optics approximation of the WKB theory applied to the incompressible ablative Rayleigh-Taylor instability, and we have found the existence of multiple branches in the unstable spectrum. The calculated cutoff wave number is also reasonably accurate for configurations with rather steep density gradients or large ablation velocity ($\Sigma \leq 1$). Although this is the first derivation of the multiple unstable branches in the presence of an equilibrium flow, this result is not surprising, as in the classical Rayleigh-Taylor instability, multiple modes also exist. However, no branch experiences a cutoff in the classical treatment, and the growth rate is monotically increasing with the mode wave number.
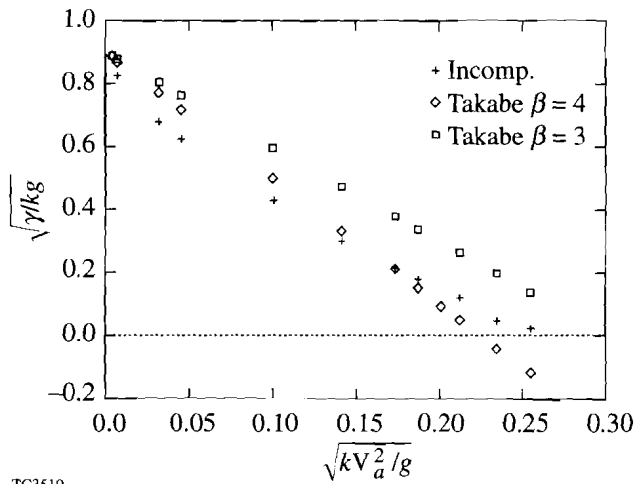
TC3519

Figure 60.8

Plot of the normalized growth rate $\sqrt{\gamma/kg}$ versus the normalized wave number $\sqrt{kV_a^2/g}$, for the incompressible model (+), Eq. (23) with $\beta = 3$ ($\square$), and Eq. (23) with $\beta = 4$ ($\Diamond$). The equilibrium parameters are $L_0 = 0.5 \ \mu m$, $g = 10^{16}$ cm/s^2, $V_a = 10^5$ cm/s, and $A = 0.95$.

REFERENCES

1. Lord Rayleigh, *Scientific Papers* (Cambridge University Press, Cambridge, England, 1900), Vol. II, p. 200.

2. S. Bodner, Phys. Rev. Lett. **33**, 761 (1974).

3. H. Takabe, K. Mima, L. Montierth, and R. L. Morse, Phys. Fluids **28**, 3676 (1985).

4. H. J. Kull and S. I. Anisimov, Phys. Fluids **29**, 2067 (1986).

5. J. H. Gardner, S. E. Bodner, and J. P. Dahlburg, Phys. Fluids B **3**, 1070 (1991).

6. K. O. Mikaelian, Phys. Rev. A **46**, 6621 (1992).

7. H. J. Kull, Phys. Fluids B **1**, 170 (1989).

8. A. B. Bud'ko and M. A. Liberman, Phys. Rev. Lett. **68**, 178 (1992).

9. C. P. Verdon, R. L. McCrory, R. L. Morse, G. R. Baker, D. I. Meiron, and S. A. Orszag, Phys. Fluids **25**, 1653 (1982).